Variation of Helical Twisting Power in Self-Assembled Sugar-Appended Schiff Base Chiral Rod−Coil Amphiphiles

Tz-Feng Lin,[†] Rong-Ming Ho,*[,†] Chien-Hung Sung,[‡] and Chain-Shu Hsu*[,‡]

Department of Chemical Engineering, National Tsing-Hua University, Hsinchu 30013, Taiwan, ROC, and Department of Applied Chemistry, National Chiao Tung University, Hsinchu 30010, Taiwan, ROC

Received August 10, 2007. Revised Manuscript Received November 14, 2007

A series of sugar-appended Schiff base chiral rod−coil amphiphiles with various alkoxy chain lengths have been synthesized in order to elucidate the variation of the helical twisting power (HTP), that is, the inverse of the pitch length, of the helical texture in the self-assembly of the amphiphiles. The HTP induced by chiral sugar in the self-assembled helical morphology was dependent upon the alkoxy chain length. Increasing the alkoxy chain length caused the self-assembled morphology to change from platelet-like texture to helical-twist morphology with varying pitch length and then revert to the platelet-like texture. This result demonstrates that the HTP reaches a maximum as the alkoxy chain length changes. The transformation from platelet-like to helical-twist morphology is induced by significant steric hindrance, when the effective size of adjacent alkoxy chains reaches the threshold of helical twisting and bending, resulting in the formation of a chiral smectic C phase. However, as the alkoxy chain length increases further, the disordering of the alkoxy chain conformation in the smectic-like layered structure may give rise to a structural imperfection that reduces the steric-hindrance effect. Eventually, the steric-hindrance effect may reach a compromise with the structural imperfection to produce a platelet-like morphology, leading to the formation of a low-order smectic phase.

Introduction

Introducing secondary forces (i.e., amphiphilicity, polarity, hydrogen bonding, coulombic interactions, van der Waals forces, metal coordination, ionic bonding, and chirality) into self-assembly of soft matter provides one convenient way to create a variety of fascinating morphologies, in a manner that biomimics natural processes.[1,2] While self-assembly of small molecules is relatively well understood, the morphologies of nanofibers, nanotubes, and nanowires obtained from self-assembly of supramolecular entities have been extensively studied. Among them, the appearance of supramolecular chirality that originates from the chiral effect has been demonstrated in self-assembled systems.[3,4] Many chiral systems, including chiral liquid crystals (LCs),[5] folded oligomers,[6] chiral dendrimers,[7] dendron rodcoils,[8] chiral homopolymers,[9] chiral block copolymers,[10] chiral counterions,[11] chiral discotic molecules,[12] dyes,[13] and chromophores,[14] have been shown to exhibit morphologies with a helical sense. These studies have focused on the design, synthesis, and characterization of various helical assemblies, such as helical ribbons, twisted fibers, and coiled tubes.

The origin of the formation of hierarchical morphologies with a helical sense is still a subject of debate. In general, the inverse of the helical pitch length is defined as helical twisting power (HTP).[15] It is well-known that control of HTP is usually accomplished by use of an enantiomeric excess

* To whom correspondence should be addressed. R.-M.H.: tel, +886-3-5738349; fax, +886-3-5715408; e-mail, rmho@mx.nthu.edu.tw. C.-S.H.: tel, +886-3-5131523; fax, +886-3-5723764; e-mail, cshsu@mail.nctu.edu.tw.

[†] National Tsing-Hua University.

[‡] National Chiao Tung University.

(1) Whitesides, G. M.; Grzybowski, B. *Science* **2002**, *295*, 2418–2421.

(2) (a) Lehn, J.-M. *Supramolecular Chemistry: Concepts and Perspectives*; VCH: Weinheim, Germany, 1995. (b) Lehn, J.-M. *Science* **2002**, *295*, 2400–2403.

(3) (a) Cornelissen, J. J. L. M.; Fischer, M.; Sommerdijk, N. A. J. M.; Nolte, R. J. M. *Science* **1998**, *280*, 1427–1430. (b) Engelkamp, H.; Middelbeek, S.; Nolte, R. J. M. *Science* **1999**, *284*, 785–788. (c) Cornelissen, J. J. L. M.; Rowan, A. E.; Nolte, R. J. M.; Sommerdijk, N. A. J. M. *Chem. Rev.* **2001**, *101*, 4039–4070.

(4) Hirschberg, J. H. K. K.; Brunsveld, L.; Ramzi, A.; Vekemans, J. A. J. M.; Sijbesma, R. P.; Meijer, E. W. *Nature* **2000**, *407*, 167–170.

(5) (a) Fuhrhop, J. H.; Helfrich, W. *Chem. Rev.* **1993**, *93*, 1565–1582. (b) Goodby, J. W.; Waugh, M. A.; Stein, S. M.; Chin, E.; Pindak, R.; Patel, J. S. *J. Am. Chem. Soc.* **1989**, *111*, 8119–8125. (c) Spector, M. S.; Price, R. R.; Schnur, J. M. *Adv. Mater.* **1999**, *11*, 337–340. (d) Jung, J. H.; John, G.; Yoshida, K.; Shimizu, T. *J. Am. Chem. Soc.* **2002**, *124*, 10674–10675.

(6) (a) Nelson, J. C.; Saven, J. G.; Moore, J. S.; Wolynes, P. G. *Science* **1997**, *277*, 1793–1796. (b) Prince, R. B.; Brunsveld, L.; Meijer, E. W.; Moore, J. S. *Angew. Chem., Int. Ed.* **2000**, *39*, 228–230.

(7) (a) Percec, V.; Glodde, M.; Bera, T. K.; Miura, Y.; Shiyanovskaya, I.; Singer, K. D.; Balagurusamy, V. S. K.; Heiney, P. A.; Schnell, I.; Rapp, A.; Spiess, H.-W.; Hudson, S. D.; Duan, H. *Nature* **1998**, *419*, 384–387. (b) Percec, V.; Dulcey, A. E.; Balagurusamy, V. S. K.; Miura, Y.; Nummelin, S.; Edlund, U.; Hudson, S. D.; Heiney, P. A.; Duan, H.; Magonov, S. N.; Vinogradov, S. A. *Nature* **2004**, *430*, 764–768.

(8) (a) Hartgerink, J. D.; Beniash, E.; Stupp, S. I. *Science* **2001**, *294*, 1684–1688. (b) Zubarev, E. R.; Pralle, M. U.; Sone, E. D.; Stupp, S. I. *J. Am. Chem. Soc.* **2001**, *123*, 4105–4106.

(9) (a) Li, C. Y.; Cheng, S. Z. D.; Ge, J. J.; Bai, F.; Zhang, J. Z.; Mann, I. K.; Chien, L.-C.; Harris, F. W.; Lotz, B. *J. Am. Chem. Soc.* **2000**, *122*, 72–79. (b) Li, C. Y.; Cheng, S. Z. D.; Weng, X.; Ge, J. J.; Bai, F.; Zhang, J. Z.; Calhoun, B. H.; Harris, F. W.; Chien, L.-C.; Lotz, B. *J. Am. Chem. Soc.* **2001**, *123*, 2462–2463. (c) Yashima, E.; Maeda, K.; Okamoto, Y. *Nature* **1999**, *399*, 449–451.

(10) (a) Ho, R.-M.; Chiang, Y.-W.; Tsai, C.-C.; Lin, C.-C.; Ko, B.-T.; Huang, B.-H. *J. Am. Chem. Soc.* **2004**, *126*, 2704–2705. (b) Chiang, Y.-W.; Ho, R.-M.; Ko, B.-T.; Lin, C.-C. *Angew. Chem., Int. Ed.* **2005**, *44*, 7969–7972. (c) Ho, R.-M.; Chen, C.-K.; Chiang, Y.-W.; Ko, B.-T.; Lin, C.-C. *Adv. Mater.* **2006**, *18*, 2355–2358.

(11) Oda, R.; Huc, I.; Schmutz, M.; Candau, S. J.; MacKintosh, F. C. *Nature* **1999**, *399*, 566–569.

10.1021/cm702252b CCC: $40.75
Published on Web 01/04/2008

of the dopant, through which the sign and size of the HTP of a compound can be modulated.[16] Several approaches based on the concept of induced chirality have been developed in order to accomplish reversible switching of guest–host materials by photochemical interconversion of diastereoisomers and photoepimerization.[17] Moreover, the change in macromolecular helicity can be manipulated by external stimuli such as temperature and solvent.[18] Theoretical predictions suggest that the helical sense of a self-assembled texture is a result of cooperative chirality competition[19] and that the connection between molecular chirality and phase chirality (i.e., pitch length) is a function of solvent, temperature, and concentration.[20] Also, the relationship between molecular chirality and HTP demonstrates the dependence of HTP on the conformational flexibility of the chiral dopant; an increase in chain flexibility leads to a lower HTP (i.e., the HTP strongly depends on the structure or stereochemistry of the chiral dopant).[21] Recently, the evolution of morphological development as a function of the alkoxy chain length in sugar-appended Schiff base chiral rod−coil amphiphiles with LC characteristics has been studied in our laboratory. Self-assembly of the chiral rod−coil amphiphiles gave rise to fascinating aggregates in aqueous solution and bulk states having stable morphologies.[22] The morphological transformation from platelet-like to helical-twist morphology was obtained simply by increasing the length of the hydrophobic chains in the chiral rod−coil amphiphiles. Therefore, sugar was suggested as a chiral entity that could initiate twisting and bending forces between molecules.

Scheme 1. Chemical Structure of the Sugar-Appended Schiff Base Chiral Rod−Coil Amphiphiles

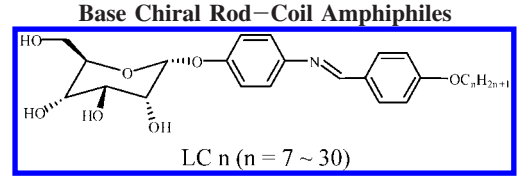

In the present work, we systematically studied the variation of HTP with alkoxy chain length in order to elucidate the origin of the twisting-and-bending mechanism in the self-assembly of chiral rod−coil amphiphiles. A further increase in the alkoxy chain length finally caused the self-assembled amphiphiles to revert from the helical-twist morphology having a maximum HTP to the platelet-like texture. This result demonstrates that the significant variation of HTP with the alkoxy chain length originates in the self-assembly of the chiral amphiphiles. Also, on the basis of structural characterization and spectroscopic analysis, we suggest that the variation in HTP results from a steric-hindrance effect and structural imperfection in the self-assembly of the chiral amphiphiles. The cause of the structural imperfection is the loss of alkoxy chain packing due to the increase in the alkoxy chain length. Consequently, molecular dispositions of self-assembled hierarchical structures are proposed in order to illustrate the variation of HTP with alkoxy chain length.

Experimental Section

Materials and Specimen Preparation. Scheme 1 indicates the general chemical structure of the sugar-appended Schiff base chiral rod−coil amphiphiles. The detailed synthetic routes combining esterification and Schiff condensation strategies have been published.[22a] In general, the Schiff base rod segment serves as a mesogenic unit to drive the LC behavior in the self-assembly process, whereas the alkoxy chains are introduced in order to decrease the rigidity of the molecular structure. The sample code indicating the alkoxy chain length (n) in the sugar-appended Schiff base chiral rod−coil amphiphiles is abbreviated as LCn (n = 7−16, 18, 22, 30).

Characterization Techniques. A Siemens D5000 1.2 kW tube X-ray generator (Cu Kα radiation) with a diffractometer was used for wide-angle X-ray diffraction (WAXD) powder experiments. The scanning angle (2θ) ranged from 1 to 35° with a scan step of 0.05° for 3 s. The diffraction peak positions and widths observed in the WAXD experiments were carefully calibrated with silicon crystals having known crystal sizes.

In order to study the HTP of hierarchical superstructures with a helical sense driven by chiral entities (i.e., the chain length effect of the hydrophobic tail), self-assembly of sugar-appended Schiff base chiral rod−coil amphiphiles was carried out in dilute solution (1 mL of THF/9 mL of H_2O). After an amount of time sufficient for the aggregation process to occur, a drop of the mixture was transferred to a carbon film for transmission electron microscopy (TEM) observations. TEM experiments were carried out using a JEOL JEM-1200CXII microscope at an accelerating voltage of 120 kV. Bright-field TEM images were obtained using the mass-thickness contrast from shadowing. Shadowing has proven useful

(12) Thunemann, A. F.; Kubowicz, S.; Burger, C.; Watson, M. D.; Tchebotareva, N.; Müllen, K. *J. Am. Chem. Soc.* **2003**, *125*, 352–356.
(13) (a) Würthner, F.; Yao, S.; Beginn, U. *Angew. Chem., Int. Ed.* **2003**, *42*, 3247–3250. (b) Lohr, A.; Lysetska, M.; Würthner, F. *Angew. Chem., Int. Ed.* **2005**, *44*, 5071–5074. (c) Rösch, U.; Yao, S.; Wortmann, R.; Würthner, F. *Angew. Chem., Int. Ed.* **2006**, *45*, 7026–7030.
(14) (a) George, S. J.; Ajayaghosh, A.; Jonkheijm, P.; Schenning, A. P. H. J.; Meijer, E. W. *Angew. Chem., Int. Ed.* **2004**, *43*, 3422–3425. (b) Ajayaghosh, A.; Vijayakumar, C.; Varghese, R.; George, S. J. *Angew. Chem., Int. Ed.* **2006**, *45*, 456–460. (c) Ajayaghosh, A.; Varghese, R.; Mahesh, S.; Praveen, V. K. *Angew. Chem., Int. Ed.* **2006**, *45*, 7729–7732.
(15) Kitzerow, H.-S.; Bahr, C. *Chirality in Liquid Crystals*; Springer: New York, 2001.
(16) (a) Kuball, H. G.; Bruning, H.; Muller, T. *J. Mater. Chem.* **1995**, *5*, 2167–2174. (b) Kuball, H. G.; Bruning, H. *Chirality* **1997**, *9*, 407–423. (c) Gottarelli, G.; Spada, G. P. *Materials-Chirality*; Green, M. M., Nolte, R. J. M., Meijer, E. W., Eds.; Topics in Stereochemistry, Vol. 24; Wiley: Hoboken, NJ, 2003.
(17) (a) Feringa, B. L.; van Delden, R. A.; Koumura, N.; Geertsema, E. M. *Chem. Rev.* **2000**, *100*, 1789–1816. (b) Ichimura, K. *Chem. Rev.* **2000**, *100*, 1847–1874.
(18) (a) Onouchi, H.; Maeda, K.; Yashima, E. *J. Am. Chem. Soc.* **2001**, *123*, 7441–7442. (b) Morino, K.; Maeda, K.; Yashima, E. *Macromolecules* **2003**, *36*, 1480–1486. (c) Hasegawa, T.; Morino, K.; Tanaka, Y.; Katagiri, H.; Furusho, Y.; Yashima, E. *Macromolecules* **2006**, *39*, 482–488. (d) Kim, H.-J.; Lee, E.; Park, H.-S.; Lee, M. *J. Am. Chem. Soc.* **2007**, *129*, 10994–10995.
(19) (a) Lifson, S.; Andreola, C.; Peterson, N. C.; Green, M. M. *J. Am. Chem. Soc.* **1989**, *111*, 8850–8858. (b) Cheon, K. S.; Selinger, J. V.; Green, M. M. *Angew. Chem., Int. Ed.* **2000**, *39*, 1482–1485. (c) Aggeli, A.; Nyrkova, I. A.; Bell, M.; Harding, R.; Carrick, L.; McLeish, T. C. B.; Semenov, A. N.; Boden, N. *Proc. Natl. Acad. Sci. U.S.A.* **2001**, *98*, 11857–11862.
(20) Sato, T.; Sato, Y.; Umemura, Y.; Teramoto, A.; Nagamura, Y.; Wagner, J.; Weng, D.; Okamoto, Y.; Hatada, K.; Green, M. M. *Macromolecules* **1993**, *26*, 4551–4559.
(21) (a) Emelyanenko, A. V.; Osipov, M. A.; Dunmur, D. A. *Phys. Rev. E* **2000**, *62*, 2340–2352. (b) Earl, D. J.; Wilson, M. R. *J. Chem. Phys.* **2003**, *119*, 10280–10288. (c) Neal, M. P.; Solymosi, M.; Wilson, M. R.; Earl, D. J. *J. Chem. Phys.* **2003**, *119*, 3567–3573. (d) Kamberaj, H.; Osipov, M. A.; Low, R. J.; Neal, M. P. *Mol. Phys.* **2004**, *102*, 431–446.
(22) (a) Sung, C. H.; Kung, L. R.; Hsu, C. S.; Lin, T.-F.; Ho, R.-M. *Chem. Mater.* **2006**, *18*, 352–359. (b) Lin, T.-F.; Ho, R.-M.; Sung, C. H.; Hsu, C. S. *Chem. Mater.* **2006**, *18*, 5510–5519.

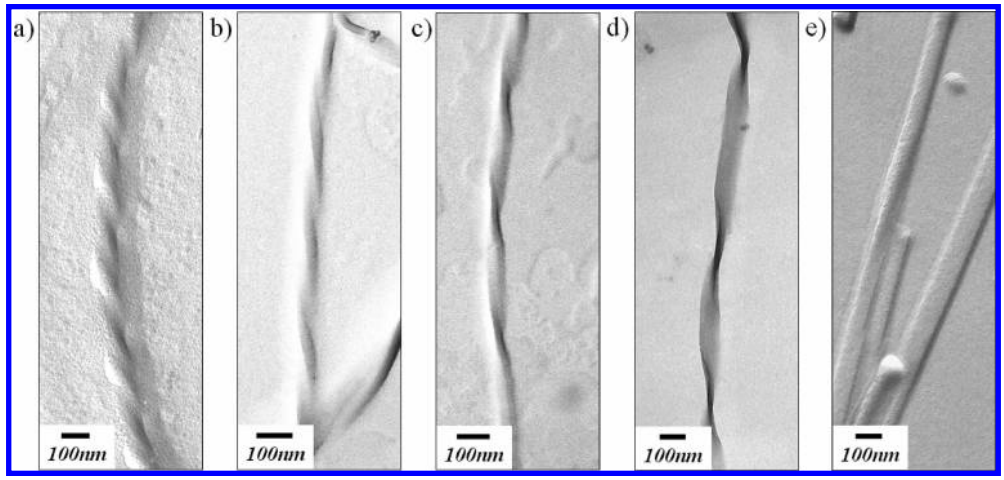

Figure 1. TEM images of the hierarchical superstructures of (a) LC14, (b) LC16, (c) LC18, (d) LC22, and (e) LC30 self-assembled in solution at ambient temperature.

in contrast enhancement by the addition of heavy metal in a vacuum evaporator. The samples first were dropped onto the carbon film and supported by a 400 mesh Cu grid that fit into the specimen holder of the microscope and then shadowed by 4/1 Pt/Pb tilted at an angle of 30° to the surface. Also, the staining procedure was accomplished by exposing the samples to the vapor of a 4% aqueous solution of RuO_4 for 3 h, in order to increase the mass-thickness contrast of positions with unsaturated bonds through bonding with RuO_4.

UV–vis absorption spectra were recorded on a Hitachi U-3300 spectrophotometer, and circular dichroism (CD) measurements were conducted on a JASCO J-720 spectrophotometer. UV–vis and CD measurements were performed in order to investigate the specific absorption bands and chiral expressions of the samples in solution. The CD curve has a convex shape in the vicinity of the maximum of a UV−vis absorption band. This kind of characteristic-shape phenomenon is known as the Cotton effect. This effect, which provides structural information, is characterized by the position, magnitude, sign, and shape of the curve. The absorption spectra of sugar-appended Schiff base chiral rod−coil amphiphiles were recorded on THF solutions (1×10^{-4} M) in quartz tubes.

Fourier-transform infrared (FTIR) spectra were recorded on a Nicolet Avatar 320 FTIR spectrometer under a nitrogen atmosphere using the KBr pellet technique; the wavenumber range was 4000−400 cm^{-1} with 1 cm^{-1} resolution, and 32 scans were collected per spectrum. Temperature-dependent FTIR measurements were conducted in order to investigate conformational transformations due to intermolecular hydrogen bonding for samples at various temperatures. The temperature control of the hot stage was calibrated to be within ±0.5 °C. The samples were studied over a temperature range of 40−260 °C and were held at each prescribed temperature for 20 min until the transformation was complete under the heating or cooling process. Overlapped vibration bands of the characteristic $-CH_2-$ symmetric and asymmetric stretching absorptions at 2850 and 2920 cm^{-1}, respectively, were resolved using the PeakFit peak-separation program (Jandel Scientific). Gaussian and Lorentzian functions were used in order to obtain the best fit.

Results and Discussion

Dependence of Amphiphile Morphology on Alkoxy Chain Length. To examine the origin of HTP in hierarchical superstructures, a series of sugar-appended Schiff base chiral rod−coil amphiphilic samples LC*n*, where *n* is the number of methylene units in the alkoxy tail ($n = 7-16$, 18, 22, 30), were designed and synthesized in this study. As we observed previously (e.g., see the TEM images of the hierarchical superstructures of LC7−LC13 in Figure 6 of ref 22a), the obvious helical twist was found once the alkoxy chain length reached a certain size (i.e., in LC9), whereas platelet-like morphology was formed for amphiphiles with short alkoxy chains (e.g., LC7). Also, the pitch length of the helical hierarchical superstructures was found to be dependent upon the alkoxy chain length. Figure 1a−e exhibits TEM observations of the hierarchical superstructures of LC14, LC16, LC18, LC22, and LC30, respectively. As shown in these images, morphological transformation from left-handed helical morphology to platelet-like texture was observed with increasing alkoxy chain length. An obvious left-handed helical twist can be identified in the self-assembled morphologies of LC14, LC16, and LC18 (Figure 1a−c). Nevertheless, as the alkoxy chain length of the amphiphilic samples was further increased, the population of the helical twist significantly decreased. Consequently, a platelet-like morphology was obtained for the amphiphilic samples with long alkoxy chains (Figure 1e).

Furthermore, the pitch length of the helical twist was strongly dependent upon the alkoxy chain length. To quantitatively measure the change in this quantity, each helical-twist pitch length was estimated by averaging the measured sizes from more than 50 TEM micrographs (Figure 2). The HTP increased to a maximum (when $n = 13$) and then decreased as the size of the alkoxy chain increased. Eventually, no helical twist was formed for the self-assembled morphology with large alkoxy chains. This behavior raised several questions: Why did the HTP reach a maximum? How did it deteriorate when the alkoxy chain length was increased? Is there a limitation on the formation of a helical twist induced by transfer of the chirality of constituent chiral entities such as sugar? To examine the mechanism for the transfer of chirality from the molecular level to the hierarchical superstructures, CD measurements were utilized first in order to confirm the appearance of helical chain conformations arising from the chiral entities. All of the synthesized amphiphiles exhibited a positive Cotton effect in the CD measurements (see Figure 3 in ref

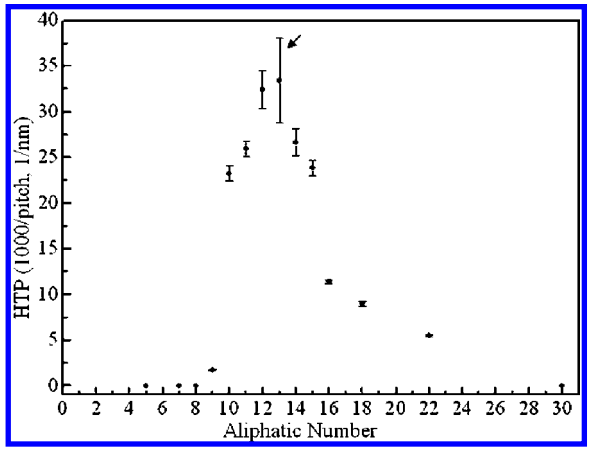

Figure 2. Dependence of HTP on the alkoxyl chain length. The arrow indicates the maximum HTP value, which occurred for LC13.

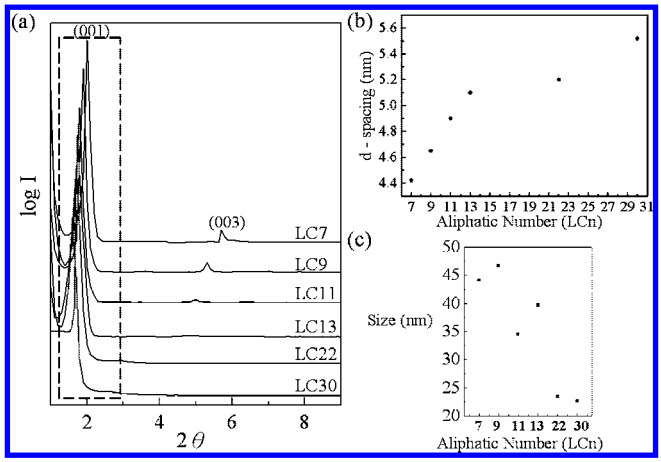

Figure 3. (a) One-dimensional WAXD profiles of sugar-appended Schiff base chiral rod−coil amphiphiles. (b) Long-period spacing determined from the primary X-ray peak as a function of the alkoxy chain length. (c) Dependence of the size of the layered structure on the alkoxy chain length; the size was determined from the width at half-maximum of the primary (001) peak using the Scherrer equation.

22a and Figure S1 in the Supporting Information for illustration), indicating the formation of a helical chain conformation. Also, the results from solid-state CD measurements (see Figure S2 in the Supporting Information) were similar to those for the solutions. These results show that the chiral expression of the primary sugar-based entity was successfully transferred to the chain-conformation level (i.e., the secondary structure) in the sugar-appended Schiff base chiral rod−coil amphiphiles, regardless of the alkoxy chain length. We thus speculate that the formation of hierarchical superstructures with a helical sense (i.e., the transfer of chirality from the chain conformation to the tertiary structure) resulted from discrepancies in chain packing for the helical chain conformation.

Identification of Amphiphile Structure. To clarify the chain packing in the hierarchical superstructures, WAXD experiments were conducted. Figure 3 shows one-dimensional WAXD profiles of LC7, LC9, LC11, LC13, LC22, and LC30. From the primary scattering peak of the X-ray experiments, well-defined diffraction at specific characteristic ratios could be identified, and the self-assembled textures were determined as layered structures. For example, in the case of LC13, a layer-to-layer *d*-spacing of 5.10 nm was

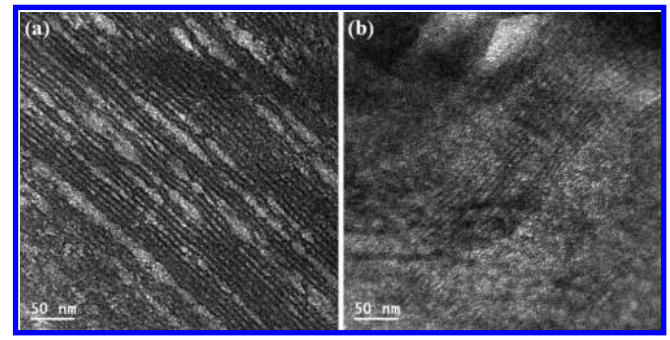

Figure 4. TEM images of (a) LC18 and (b) LC30. Samples were stained with RuO_4. Bright domains correspond to alkoxy chain regions. Layer sizes of ~6 and ~9 nm for LC18 and LC30, respectively, can be identified.

determined from the primary X-ray scattering peak, using the expression $\lambda = 2d \sin \theta$. On the basis of previous studies,[22b] the assumption of bilayered texture is consistent with the fact that the layer-to-layer *d*-spacing indeed increased with the alkoxy chain length, as evidenced by the shift of the primary X-ray peak to smaller angles with increasing *n*. However, the layer-to-layer *d*-spacing gradually deviated from a linear relationship with the alkoxy chain length as the number of methylene units in the alkoxy tail increased (Figure 3b). Also, the decreasing intensity of the (003) reflection [normalized to the (001) reflection] with increasing alkoxy chain length could be clearly seen, reflecting a possible loss of packing order for the layered structure. As in the case of the intensity of the (003) reflection, a significant decrease in the size of the layered structures (from 44.1 nm for LC7 to 22.6 nm for LC30) with increasing alkoxy chain length was found (Figure 3c). The variation in size could also be observed by TEM (Figure 4). The TEM images show that the increase in the length of the flexible alkoxy chain causes imperfection in the layered structure that results in misalignment of the rigid cores, leading to the deviation from a linear increase in *d*-spacing and also to the decrease in the size of the layered structures. Eventually, the effect of steric hindrance is diminished by the misalignment of the rigid cores due to the loose packing of the chiral entities.

In order to further examine the imperfection of layered structure, FTIR experiments to identify variations in the chain conformations of the alkoxy tails were performed. As shown in Figure 5, the characteristic vibration band at ~3330 cm^{-1}, corresponding to intermolecular hydrogen-bond formation attributed to the aggregation of sugar entities in the layered structure, decreased with increasing alkoxy chain length. This suggests that the structural imperfection was indeed enhanced by the increase of the alkoxy chain length, since the probability of forming intermolecular hydrogen bonds determines the packing efficiency of the self-assembled layered structure. In addition, as in situ FTIR measurements (Figure 6) show, the intensity attributed to the intermolecular hydrogen-bond formation decreased with increasing temperature because of the reduction in packing efficiency. Moreover, the characteristic $-CH_2-$ symmetric and asymmetric stretching bands at 2850 and 2920 cm^{-1}, respectively, can also be identified. The intensities of these peaks gradually increase with the alkoxy chain length because of the

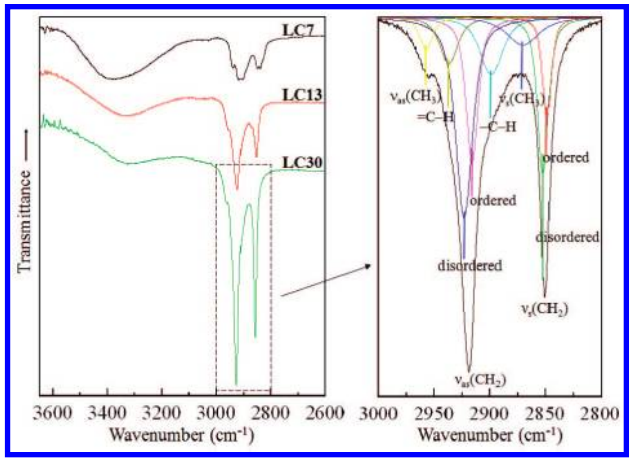

Figure 5. (Left) FTIR spectra of LC7, LC13, and LC30 at room temperature, normalized to the benzene-ring peak at 1605 cm^{-1}. Values of ν(OH): LC7, ~3391 cm^{-1}; LC13, ~3321 cm^{-1}; LC30, ~3314 cm^{-1}. (Right) Deconvolution of the overlapping vibrational bands between 2800 and 3000 cm^{-1}. Respective values of $\nu_{as}(CH_2)$ and $\nu_s(CH_2)$: LC7, ~2917 and ~2848 cm^{-1}; LC13, ~2923 and ~2853 cm^{-1}; LC30, ~2925 and ~2857 cm^{-1}.

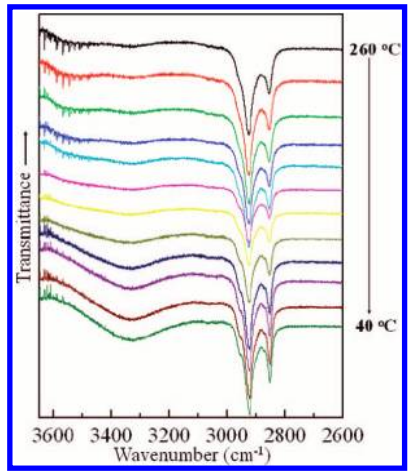

Figure 6. Temperature dependence of FTIR spectra for LC13 obtained during cooling. Similar spectroscopic results were also found for LC7 and LC30.

increasing number of $-CH_2-$ groups in the chain. The characteristic vibrational bands between 2800 and 3000 cm^{-1} can be deconvoluted into eight vibrational bands, located at 2850, 2855, 2870, 2900, 2918, 2927, 2937, and 2959 cm^{-1}. These peaks correspond to the following C−H stretch modes: all-trans alkoxy chain methylene [$\nu_s(CH_2) \approx$ 2846–2850 cm^{-1} and $\nu_{as}(CH_2) \approx$ 2916–2920 cm^{-1}]; disordered alkoxy chain methylene [$\nu_s(CH_2) \approx$ 2854–2856 cm^{-1} and $\nu_{as}(CH_2) \approx$ 2924–2928 cm^{-1}]; methyl [$\nu_s(CH_3) \approx$ 2872 cm^{-1} and $\nu_{as}(CH_3) \approx$ 2962 cm^{-1}]; alkyl [$\nu(-C-H) \approx$ 2900 cm^{-1}]; and vinyl [$\nu(=C-H) \approx$ 2937 cm^{-1}].[23] Of particular importance are the vibration bands at 2848 and 2918 cm^{-1} assigned to the ordered all-trans conformation and the bands at 2856 and 2924 cm^{-1} assigned to the disordered alkoxy chain conformation. These assignments make possible the determination of the relative proportions of the ordered all-trans and disordered alkoxy chain conformations by deconvolution of the overlapping absorptions of both vibrational modes.

(23) Silverstein, R. M.; Bassler, G. C.; Morrill, T. C. *Spectrometric Identification of Organic Compounds*, 5th ed.; John Wiley: New York, 1991.

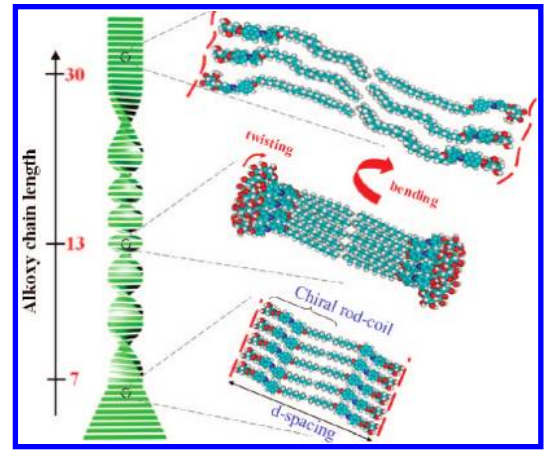

Figure 7. Hypothetical model of the effect of the alkoxy chain length on self-assembled ordered layered structures.

Consistent with the expected variation in chain conformation with alkoxy chain length, the relative proportion of the disordered alkoxy chain increased with the alkoxy chain length, rising from ~21% in LC7 to ~50% in LC13 and finally to ~66% in LC30, as determined on the basis of the changes in both the symmetric and asymmetric $-CH_2-$ vibrations (see Figures S3−S5 in the Supporting Information for detailed deconvolution results). As a result, the structural imperfection can be directly identified by the FTIR results for the $-CH_2-$ vibration bands, which provide a quantitative analysis of the extent of disordered alkoxy chain conformation as a function of the alkoxy chain length.

Molecular Dispositions of HTP Variation. Figure 7 illustrates the effect of the alkoxy chain length on the structure of the self-assembled ordered layer. Using TEM, we observed interesting morphological evolution in the sugar-appended Schiff base chiral rod−coil amphiphiles as the alkoxy chain length was varied. Increasing the alkoxy chain length caused the self-assembled morphology to change from a platelet-like texture to a helical-twist morphology with varying pitch length and then revert to the platelet-like texture. This result demonstrates the significant variation of HTP with the alkoxy chain length; the maximum HTP occurred in the self-assembly of LC13. Also, ordered layered structures can be formed in the self-assembled textures, as identified by X-ray diffraction results. The internal structures of the hierarchical superstructures with and without helix sense both possessed smectic-like bilayer character having parallel packed alkoxy groups as well as loosely packed sugar entities instead of interdigitated molecular dispositions, according to diffraction analyses of the *d*-spacing (as illustrated in Figure 3b).[22a] We thus speculate that the variation of HTP with the alkoxy chain length is attributed to the change in molecular chain conformation, even though all of them appeared with smectic-like bilayer character. Consequently, the population of disordered alkoxy chain conformations might be enhanced by the introduction of longer alkoxy chains in order to cause structural imperfection (i.e., loose packing of alkoxy chains, as illustrated) in the layered structure. The structural imperfection in the layered structure was elucidated by the FTIR results, which showed that the formation of intermolecular hydrogen bonding attributed to the aggregation of sugar entities in self-assembly gradually decreased as the

alkoxy chain length increased. Also, as the X-ray results demonstrated, the structural imperfection may cause the reduction in the size of the layered structures.

Therefore, for short alkoxy chain lengths (i.e., LC5 and LC7), the self-assembled morphology (i.e., a platelet-like morphology) exhibits typical liquid-crystalline bilayered texture as a smectic A (SmA) phase.[22b] Nevertheless, mixed morphology, including both platelet-like and left-handed helical-twist morphologies, can be observed (see Figure 6b of ref 22a). The morphological transformation from platelet-like to helical-twist morphology is attributed to HTP induced by steric hindrance, when the effective size of adjacent alkoxy chains reaches the threshold of twisting and bending required for the formation of helical morphology. With an increase in the alkoxy chain length (i.e., in going from LC11 to LC13), the increase of HTP thus corresponds well with the change of alkoxy chain length at which a chiral smectic C (SmC*) phase is formed as a result of induction of twisting and bending in the molecular packing.[22b] However, the disordering of the alkoxy chain conformation in the layered structure may give rise to a structural imperfection that reduces the steric hindrance effect. As a result, for long alkoxy chains (i.e., LC14 to LC22), the deterioration of ordered layered structure size thus leads to the decrease of HTP, although the structure still appears as a SmC* phase (see Figure S6 in the Supporting Information). Moreover, the steric-hindrance effect may reach a compromise with the structural imperfection so that a platelet-like morphology is formed (as in LC30, for instance), leading to the formation of a low-order smectic phase, as evidenced by polarized-light microscopy (PLM) observations (see Figure 8). In addition to the sugar-based compounds, peptide-based samples have also been synthesized and examined in our studies (not shown).[24] Similar results for the variation of HTP attributed to control over the pitch of supramolecular helices have also been observed.[25]

Conclusions

The helical twisting power induced by chiral sugar in the self-assembled helical morphology is dependent upon the alkoxy chain length. Increasing the alkoxy chain length caused the self-assembled morphology to change from a platelet-like texture to a helical-twist morphology with varying pitch length and then revert to the platelet-like texture. This result demonstrates that significant variation of HTP with the alkoxy chain length can be found in the self-assembly of the chiral amphiphiles, with the maximum HTP occurring in the self-assembly of LC13. The variation in the HTP is the result of both steric hindrance and structural imperfection in the self-assembly of the chiral amphiphiles. Moreover, the internal structures of the hierarchical superstructures with and without helix sense both possessed the smectic-like bilayered character having parallel packed alkoxy groups. We thus suggest that the decrease of HTP with alkoxy chain length can be attributed to the change in molecular-chain packing of the alkoxy tails.

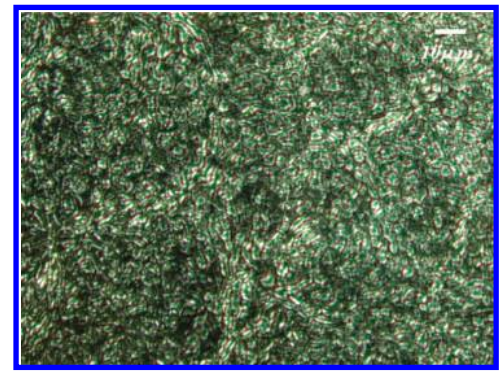

Figure 8. PLM image of LC30 obtained at room temperature. A similar result is observed at 125 °C.

Acknowledgment. Funding from the National Science Council of Taiwan is gratefully acknowledged. Our appreciation is extended to Ms. P.-C. Chao and Ms. S.-Y. Lee of the Regional Instruments Centers at National Chung Hsing University and National Sun Yat-Sen University for their help in the TEM and X-ray scattering experiments, respectively.

Supporting Information Available: CD spectra, typical FTIR spectra and peak determination results, and PLM images for selected members of the series of sugar-appended Schiff base chiral rod−coil amphiphiles (PDF). This material is available free of charge via the Internet at http://pubs.acs.org.

CM702252B

(24) Detailed studies are still in progress and will be published elsewhere.
(25) Li, L.-S.; Jiang, H.; Messmore, B. W.; Bull, S. R.; Stupp, S. I. *Angew. Chem., Int. Ed.* **2007**, *46*, 5873–5876.